Pflügers Archiv - European Journal of Physiology (2026) 478:57
https://doi.org/10.1007/s00424-026-03187-8

RESEARCH

Inhibition of (interstitial) $P2Y_6$ receptors attenuates fibrosis progression

Lena Marie Süß[1] · Anna Petzendorfer[1] · Minh Linh Tran[1] · Bettina Firmke[2] · Anja Süß[1] · Richard Warth[1] · Katharina Anna-Elisabeth Broeker[2] · Anna-Lena Forst[1]

Received: 18 March 2026 / Revised: 27 May 2026 / Accepted: 2 June 2026

Abstract

Chronic kidney disease (CKD) affects over 850 million people worldwide and is characterized by progressive renal fibrosis driven by activated interstitial fibroblasts. Signaling by extracellular nucleotides and P2 receptors plays an important role in renal pathophysiology, yet its contribution to fibroblast activation and fibrosis remains poorly understood. Here, we investigated the expression and function of $G_{q/11}$-coupled P2Y receptors in renal interstitial fibroblasts and their involvement in experimental kidney fibrosis. Using highly selective RNA in situ hybridization, we detected $P2Y_1$ (*P2ry1*) and $P2Y_6$ (*P2ry6*) receptor expression in interstitial fibroblasts. Notably, $P2Y_6$ expression was markedly upregulated in several experimental mouse models of renal fibrosis. Functional assays in primary cultured renal fibroblasts confirmed $G_{q/11}$-coupled P2Y receptor activity, as evidenced by transient intracellular Ca^{2+} elevations upon nucleotide stimulation. Primary cultured renal fibroblasts exhibited enhanced migration in response to extracellular uridine diphosphate (UDP). To assess the contribution of interstitial $P2Y_6$ receptors to fibrosis progression, we employed an adenine-induced nephropathy model with or without the selective $P2Y_6$ antagonist MRS2578. Pharmacological inhibition of $P2Y_6$ significantly reduced the mRNA expression of the myofibroblast marker α-smooth muscle actin and collagen I. Collectively, these findings suggest that upregulated $P2Y_6$ receptor signaling promotes the transition of resident interstitial cells into myofibroblasts during renal fibrosis, likely by modulating fibroblast migration. Inhibition of $P2Y_6$ signaling could represent a new strategy for reducing excessive renal fibrosis.

Keywords $P2Y_6$ (*P2ry6*) receptor · Interstitial fibroblasts · Renal fibrosis · MRS2578

Introduction

Renal fibrosis represents a common pathological end-stage of chronic kidney disease (CKD) and is a major contributor to progressive loss of kidney function. It is characterized by excessive accumulation of extracellular matrix (ECM) components such as collagens, fibronectin, and tenascins, leading to structural alterations and ultimately irreversible damage to the renal parenchyma and loss of endocrine functions [1–3]. Increased ECM production primarily originates from myofibroblasts, which can transdifferentiate from several cell types, including fibroblasts, monocytes, tubular epithelial cells, and endothelial cells [4–7]. Although the relative contribution of these cell types to the myofibroblast population may vary depending on the experimental model, growing evidence identifies platelet-derived growth factor receptor-β (PDGFR-β)-expressing resident fibroblasts and pericytes as the main precursors of myofibroblasts in human

This study reveals the role of the $P2Y_6$ receptor (*P2ry6*) in fibrotic processes in the kidney. $P2Y_6$, a $G_{q/11}$ protein-coupled UDP-sensitive receptor, is expressed in renal interstitial PDGFR-β-positive cells and macrophages. Its pharmacological inhibition significantly reduces fibrosis in the mouse adenine nephropathy model. Blocking $P2Y_6$ therefore represents a promising therapeutic strategy for kidney diseases characterized by excessive scarring.

✉ Anna-Lena Forst
anna-lena.forst@ur.de

[1] Medical Cell Biology, University of Regensburg, Universitätsstraße 31, D-93053 Regensburg, Germany

[2] Institute of Physiology, Physiology I, University of Regensburg, Universitätstr. 31, D- 93053 Regensburg, Germany

Published online: 17 June 2026

kidneys [2, 8, 9]. Macrophage-to-myofibroblast transition also contributes to interstitial fibrosis in chronic renal allograft injury [10, 11].

Differentiation of PDGFR-β-positive cells into myofibroblasts is a multifactorial process involving numerous signaling pathways, including the well-studied transforming growth factor-β1 (TGF-β1) and angiotensin II [3, 12, 13]. In addition to these established profibrotic mediators, recent studies implicate extracellular nucleotides as important regulators of fibroblast homeostasis. Nucleotide release is likely regulated and facilitated by several mechanisms, including vesicular or lysosomal exocytosis and channel-mediated release via connexins or pannexins during cellular stress such as mechanical strain or hypoxia. These nucleotides act as danger-associated molecular patterns (DAMPs) in both paracrine and autocrine signaling [14–17]. Extracellular nucleotides act through specific P2 and P1 receptors [15, 18–21]. While P1 receptors bind adenosine, P2 receptors are activated by purine and pyrimidine nucleotides and can be further subdivided into P2Y receptors and P2X receptors. P2X receptors function as non-selective cation channels, while the P2Y receptor isoforms are G protein-coupled receptors that are activated with differing selectivity by adenosine triphosphate (ATP), adenosine diphosphate (ADP), uridine triphosphate (UTP), and uridine diphosphate (UDP) [22, 23]. P1 and P2 receptor expression has been reported in all segments of the nephron and renal vasculature. Epithelial cells often express multiple receptor subtypes at both the apical and basolateral cell membranes [15, 19], yet little is known about expression of these receptors in interstitial cells.

Besides P1 and P2 receptors, other components of the purinergic signaling pathway include ectonucleases like CD39 (*ENTPD1*), which catalyze sequential hydrolysis of tri- and diphosphates to monophosphates or CD73 (*NT5E*) converting adenosine monophosphate to adenosine. Notably, CD73 is another marker for interstitial fibroblasts that is expressed by appr. 60% of PDGFR-β-positive cells indicative of active purinergic activity in the proximity of interstitial cells [8]. It is well known that important physiological functions such as cell proliferation and growth, energy metabolism, and transepithelial flow are influenced by extracellular nucleotides. However, knowledge about the significance of these signaling pathways in interstitial cells of the kidney is still incomplete.

In the pathophysiological setting, renal P2R receptor activation occurs in diverse inflammatory and non-inflammatory diseases including hypertension [19, 24–26], transplant rejection [21] and polycystic kidney disease [20, 27]. The influence of P1 or P2 receptors on the development of renal fibrosis has been the subject of several studies with context-depending and sometimes controversial results: Adenosine signaling through P1 receptors, particularly A_{2A} and A_{2B}, exerted protective as well as profibrotic effects [21]. Abrogating $P2X_7$ receptor signaling, which is known to promote inflammation and fibrotic remodeling via NLRP3 inflammasome activation and IL-1β release, promised the most therapeutic potential in murine fibrotic disease models so far [24, 25, 28, 29]. Despite these promising pre-clinical results however, the beneficial effect in completed phase 2 clinical trials was disappointingly mild [15].

While the current research focuses on the inhibition of inflammatory cells via blockage of $P2X_7$, we were interested in the potential role of P2Y receptors of interstitial cells in fibrosis progression. In the present study, we analyzed the expression and functionality of murine $G_{q/11}$ protein-coupled receptors ($P2Y_1$, $P2Y_2$, $P2Y_4$ and $P2Y_6$) in healthy and fibrotic murine kidneys. Additionally, we subjected mice to different experimental models of kidney fibrosis to elucidate the therapeutic potential of specific $P2Y_6$ signaling on fibrosis progression.

Results

Renal mRNA expression of $G_{q/11}$ protein-coupled P2Y receptors

To determine which murine $G_{q/11}$ protein-coupled *P2ry* (*P2ry1*, *P2ry2*, *P2ry4*, *P2ry6*) receptors are expressed in interstitial PDGFR-β-positive cells of the kidney, multiplex RNA *in- situ* hybridizations on adult murine cross-sections were performed. Interstitial cells were marked using a *Pdgfrb*-probe. Note the low abundance of all P2Y-receptor mRNA compared to *Pdgfrb*, which is typical for many $G_{q/11}$ protein-coupled receptors [30]. *P2ry* expression was seen throughout all kidney zones (Fig. 1). *P2ry1* was predominantly found in cells of the glomerulus, proximal tubular cells, urothelium and PDGFR-β-positive interstitial cells. *P2ry2* was observed in (proximal) tubules, with increasing expression towards the medulla. *P2ry4* expression was extremely low. Few *P2ry4* signals were seen in cells of the glomerulus, (proximal) tubular cells and interstitial cells although mRNA expression seemed to be as low as one copy per cell. Interestingly, *P2ry6* was the only receptor strongly enriched in PDGFR-β-positive fibroblasts, with additional localization in proximal tubules (1–2 mRNA copies per cell).

Active P2Y receptor-mediated signaling in cultured renal fibroblasts

To verify the functionality of the P2Y receptors in interstitial fibroblasts, we isolated PDGFR-β-positive interstitial cells expressing a membranous GFP construct under the control of

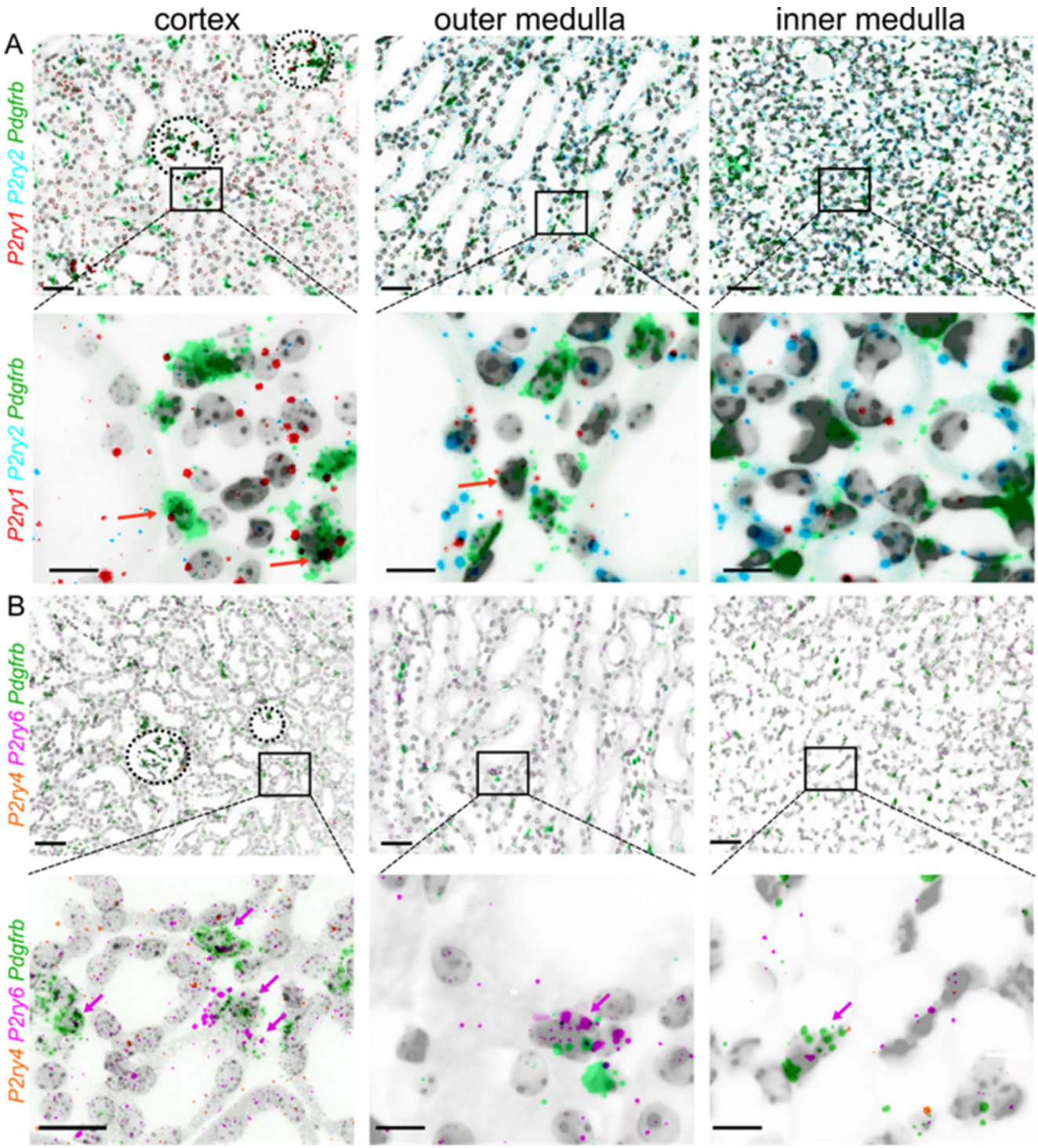

Fig. 1 RNA expression of $G_{q/11}$ protein-coupled P2Y receptors in murine kidneys. Zonal details showing the co-expression of *P2*ry1 (red), *P2ry2* (cyan) (**A**), *P2ry4* (orange), *P2ry6Y2ry6* (pink) (**B**) and the interstitial fibroblast marker *Pdgfrb* (green) in transverse murine kidney sections using RNAscope. The upper panel in (**A**) and (**B**) shows details from the cortex, outer medulla and inner medulla of a control mouse (scale bar=50 µm). The lower panel shows the respective details (scale bar=20 µm). Colored arrows indicate double *Pdgfrb*- and rsepective *P2yr*-positive fibroblasts

the *Pdgfrb*-promotor from PDGFR-β $Cre^{ERT/2}$ mTmG mice using fluorescence-activated cell sorting (FACS). After cultivation, we verified expression of the $G_{q/11}$ protein-coupled P2Y receptors using mRNA in-situ hybridization (Supplementary Fig. 1). Subsequently, fibroblasts were loaded with the Ca^{2+}-indicator Fura-2 and active $G_{q/11}$ protein signaling was investigated using videomicroscopic imaging. Cells responded to superfusion with the nucleotides ATP, ADP, UTP or UDP with transiently increased oscillating Ca^{2+}-signals indicative of intracellular store release (Fig. 2). P2X involvement was excluded by removal of extracellular Ca^{2+}, which did not affect ATP-mediated cytosolic Ca^{2+}-signaling (Supplementary Fig. 2A). To identify active P2Y isoforms, we applied selective antagonists where available. We observed that ADP-mediated signaling could be significantly reduced, but not completely suppressed, by specific inhibition of the ADP-sensitive $P2Y_1$ receptor using MRS2179 (Fig. 2B). Similarly, UDP-mediated responses were markedly attenuated by MRS2578, an irreversible covalent antagonist of $P2Y_6$ that inactivates the receptor by modifying a critical cysteine residue, leading to internalization and degradation [31, 32] (Fig. 2C). Notably, neither MRS2179 nor MRS2578 caused nonspecific inhibition of Ca^{2+} responses to other nucleotides, whereas the broad-spectrum P2 receptor antagonist suramin suppressed all nucleotide-induced Ca^{2+} transients (Supplementary Fig. 2).

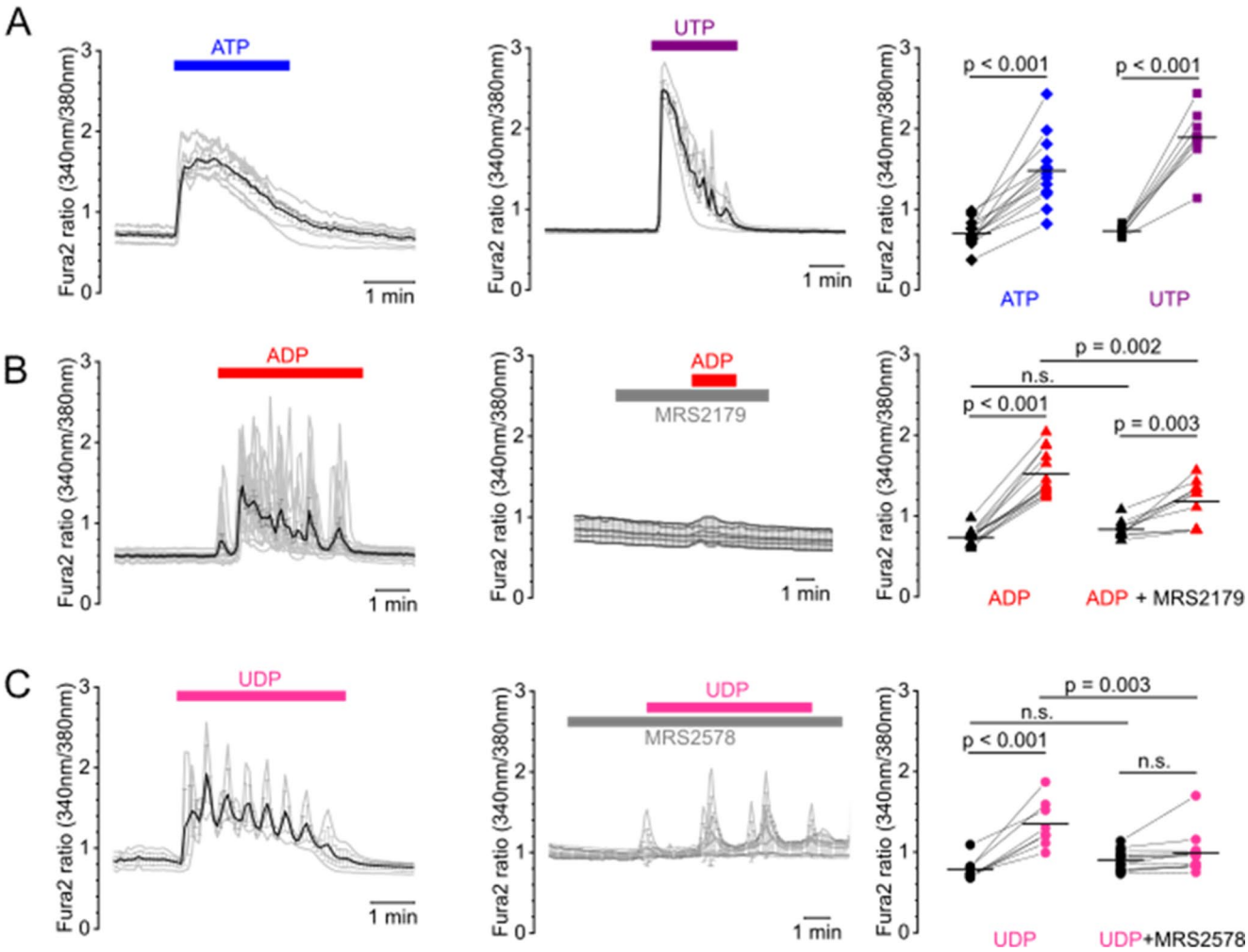

Fig. 2 Active P2Y receptor-mediated signaling in cultured renal fibroblasts. (A) FACS-sorted, cultivated murine renal fibroblasts were loaded with the Ca^{2+}-indicator Fura2 and superfused with agonists and antagonists of P2Y receptors. (**A**) Representative trace of single cells (grey lines) superfused with 100 µM ATP (left) or UTP (middle). Black lines represent the mean traces per dish. Summary on the right indicates basal (black) and respective maximal Ca^{2+} transients (colored symbols) under activation. Each connected dot represents the mean of one dish. (**B**, **C**) Left panel shows a representative trace of cells superfused with 100 µM ADP (**B**) or UDP (**C**). Middle panel depicts a representative trace in the presence of 5 µM of specific $P2Y_1$ inhibitor MRS2179 (**B**) or 5 µM of the specific $P2Y_6$ inhibitor MRS2578 (**C**). Summary on the right indicates basal (black) and respective maximal Ca^{2+}-transients (colored symbols) of the respective measurements. Each condition was tested at least with three different cell lines

$P2Y_6$ receptors are upregulated in renal fibrosis models To analyze the role of $G_{q/11}$ protein coupled P2Y receptors in fibrosis, we re-examined cDNA (generated in previous study [3] from whole kidney lysates of different experimental kidney fibrosis models including adenine nephropathy (adenine) and unilateral ureteral obstruction (UUO) using quantitative PCR (Supplementary Fig. 3). *P2ry1* mRNA normalized to the housekeeping gene *actb* was significantly downregulated from 1.00±0.28 to 0.69±0.45 in the UUO model (p=0.018), but not in the adenine-induced nephropathy (p=0.268), while *P2ry2* mRNA was significantly downregulated from 1.00±0.3 in the UUO model (p=0.008) but significantly upregulated in the adenine-induced nephropathy from 1.00±0.46 to 1.64±0.22 (p=0.042) (Supplementary Fig. 3). We could not reproducibly amplify *P2ry4* mRNA probably due its low expression as evidenced by the RNA *in situ* hybridization experiments. Normalized *P2ry6* was increased in both fibrosis models from 1.00±0.53 to 1.85±1.26 in the UUO model (p=0.032) and from 1.00±0.70 to 3.83±1.39 in the adenine model (p=0.002). These results are indicative for distinctively different regulation of $G_{q/11}$PCR P2Y-receptor isoforms in renal disease progression with $P2Y_6$ upregulation being a common entity. To analyze the localization of renal $P2Y_6$ receptors under fibrotic conditions, we conducted a reversible unilateral ureter obstruction (rUUO) for five days whereafter the fibrosis progression was continued for two weeks. Similarly, adenine-induced nephropathy was induced by a high adenine diet for three weeks whereafter kidneys were harvested and analyzed using RNA in situ hybridization with specific *P2ry6* and *Pdgfrb*-probes (Fig. 3). Automated quantitative image analysis of cortical *P2ry6* signals revealed that, regardless of the disease model, the $P2_6$-positive area was upregulated from 3.3±0.5% to 5.9±1.5% in the rUUO model (p=0.042) where the contralateral kidney served as internal control, and from 4.5±0.9% to 11.3±4.3 in the adenine model (p<0.001) (Fig. 3D). Interestingly, *P2ry6*-positive signal was strongly enriched in the interstitial space but not exclusively co-localized with *Pdgfrb*. Besides *Pdgfrb*-co-hybridization, we observed a strong co-localization with the macrophage marker F4/80 (*Adgre1*) that also increased in the cortical areas from 1.9±0.6% to 4.1±1.3% in the rUUO model (p=0.032) and from 1.0±0.3% to 7.6±3.4% in the adenine model (p<0.001). In contrast, *Pdgfrb*-positive area did not significantly change in the disease models.

Pharmacological inhibition of $P2Y_6$ receptors in fibrosis progression To assess the role of $P2Y_6$ in the development of renal fibrosis, we inhibited $P2Y_6$ receptors using MRS2578 in adenine-induced nephropathy. Fibrosis progression was assessed by immunofluorescent staining of α-smooth muscle actin (αSMA) on transverse murine kidney slices. The percentage of αSMA-positive area was determined automatically using a thresholding approach (Fig. 4). Adenine diet resulted in statistically significant increase of cortical αSMA-positivearea compared to control kidneys (p=0.002). Pharmacological inhibition of $P2Y_6$ using MRS2578 significantly attenuated fibrosis progression as estimated by αSMA immunostaining from 1.00±0.31 to 0.53±0.16 (p=0.004) in the adenine-induced model, with the mean value for vascular αSMA in healthy control kidneys being 0.29±0.14. Additionally, the mRNA expression of markers of fibrosis was examined using qPCR. As depicted in Fig. 4D, collagen I (*Col1a1*) mRNA levels were significantly decreased in MRS2578 treated animals compared to animals receiving vehicle injections and adenine enriched food. $P2Y_6$ (*P2ry6*) mRNA levels were also examined. They were upregulated in the adenine-fed animals but not significantly affected by MRS2578.

$P2Y_6$ receptor activation promotes migration of fibroblasts Given the expression of $P2Y_6$ in interstitial cells and macrophages, we wondered what effect $P2Y_6$ activation has on these cells. Macrophages are known to be activated in the presence of the $P2Y_6$ agonist UDP leading to a pro-inflammatory, chemokine-releasing phenotype [33, 34]. Given that UDP acts as a danger associated molecular pattern in the interstitium, we speculated that PDGFR-β-positive fibroblasts might be drawn to the site of UDP release. Therefore, we examined migration of serum-starved cultured FACS-sorted PDGFR-β-positive fibroblasts in a wound healing assay, where a confluent monolayer of fibroblasts was scratched with a pipette tip and photographed immediately and 48 h after the scratch formation. Cells at the 48 h time point were additionally stained using the nuclear marker HOE33342 and migration of cells into the scratch was automatically analyzed by counting nuclei of invading cells (Fig. 5). Migration was assessed by normalizing to invading cells in control conditions. In the presence of 30 µM UDP, 14.6±13.1% more cells migrated into the scratch compared to control cells (p=0.003) while the addition of 5 µM MRS2578 abolished the effect of UDP (-7.0±15.1%, p=0.303). The addition of MRS2578 alone also significantly decreased migration by 20.3±6.3% (p=0.002). Of note, we did not observe altered proliferation of FACS-derived murine fibroblasts due to UDP or MRS2578 stimulation (Fig. 3C).

Discussion

Renal fibrosis is a central pathological feature of chronic kidney disease (CKD), ultimately leading to irreversible loss of renal function. More than 850 million people

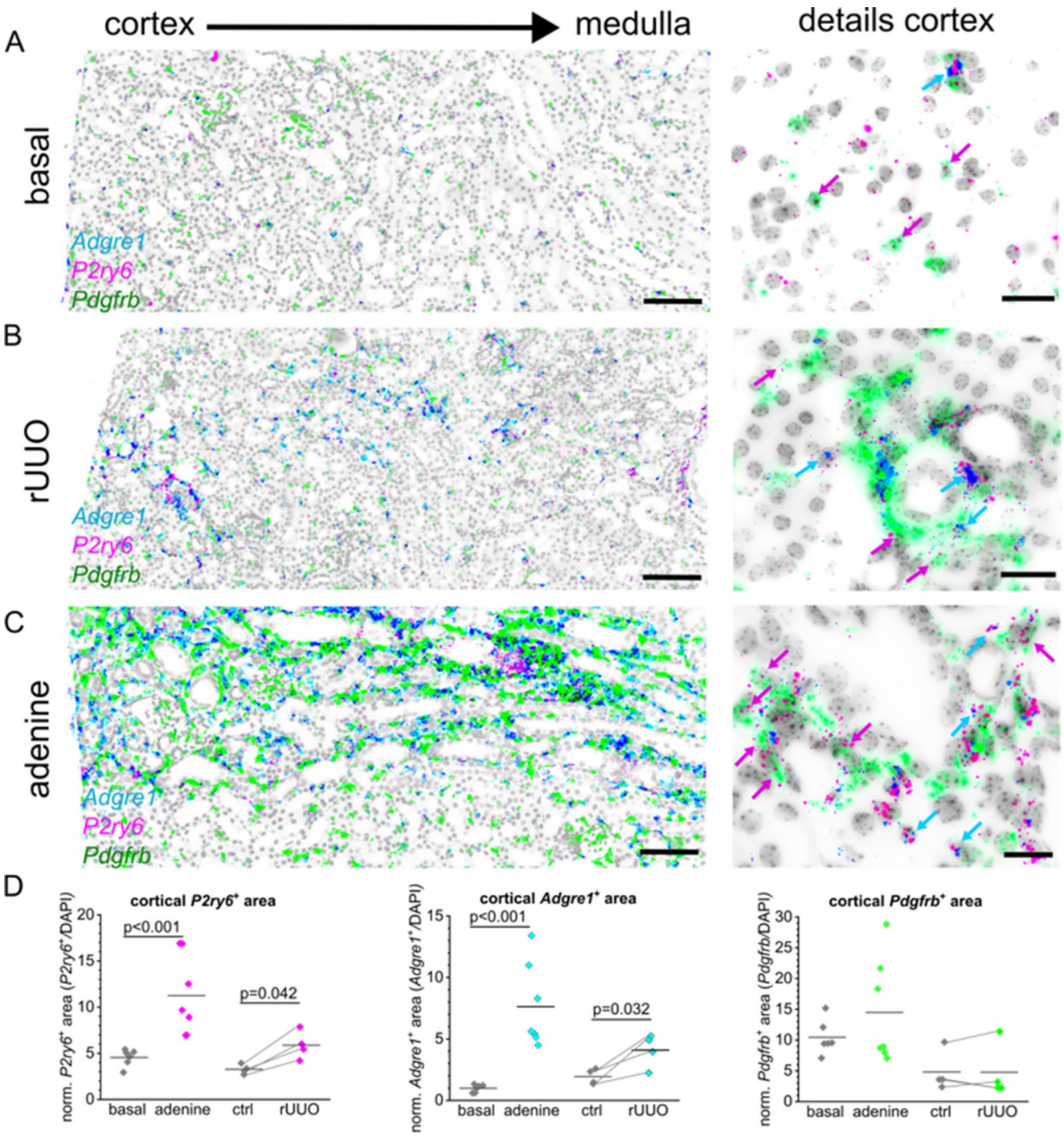

Fig. 3 *P2ry6* is regulated in renal fibrosis models. Representative pictures on the left show the co-expression of *P2ry6* (pink), the macrophage marker *Adgre1* (cyan) and the interstitial fibroblast marker *Pdgfrb* (green) in transverse murine kidney sections using RNAscope (Scale bar = 100 µm), while close-ups on the right present cortical details (scale bar = 20 µm) of a control mouse (A). Representative fibrotic kidney sections from either a mouse subjected a reversible unilateral ureter obstruction (rUUO), or adenine-induced nephropathy are depicted in (**B**) or (**C**) respectively. (**D**) Automated images analysis or cortical *P2ry6-positive* (left), *Adgre1-positive* (middle) or *Pdgfrb*-positive (right) are normalized to total analyzed area. Each dot represents one mouse. In rUUO mice, contralateral kidneys (ctrl) were use as control and respective damaged kidney are linked by a line

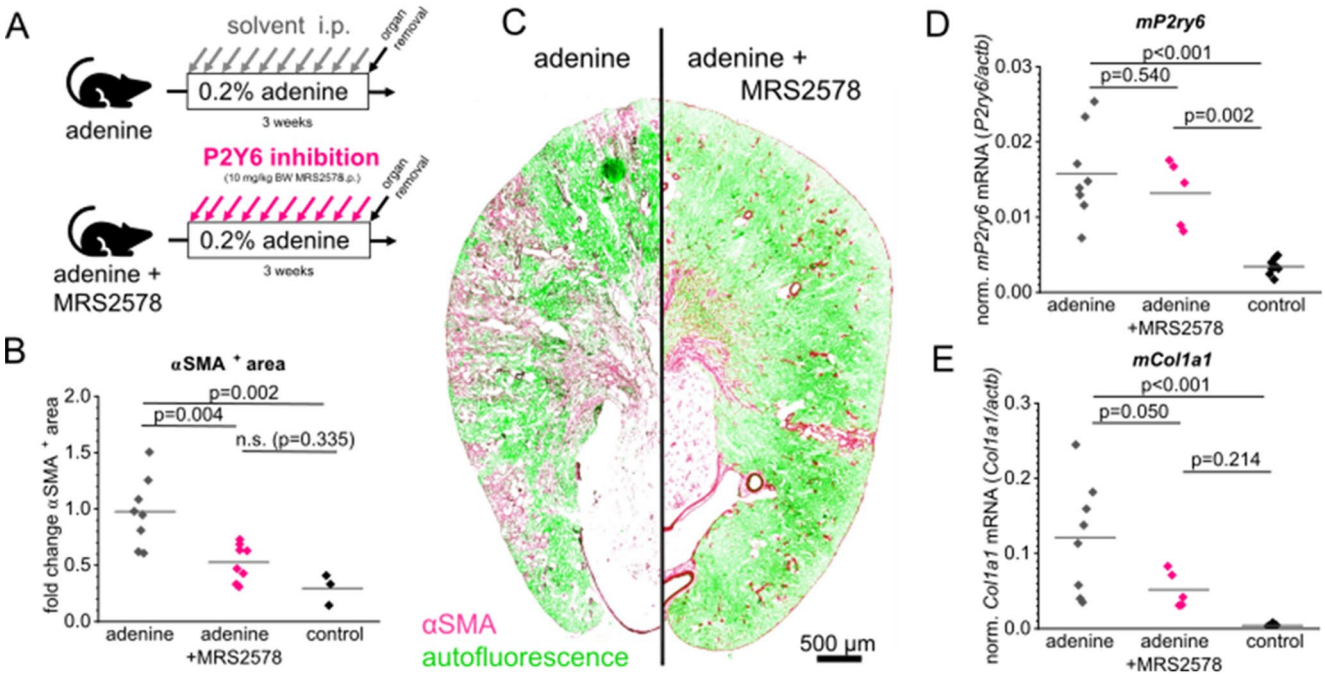

Fig. 4 Inhibition of $P2Y_6$ signaling a mice attenuates fibrosis progression. (**A**) To induce a renal fibrosis, male mice were fed a high adenine diet (0.2% adenine) for three weeks. During this period, one group of animals was injected i.p. with 10 mg/kg BW of the specific $P2Y_6$ inhibitor MRS2578 (marked "adenine + MRS2578"). The group marked with "adenine" received a diet enriched with adenine and injections of the vehicle. The extent of fibrosis was automatically analyzed using transverse murine kidney sections of each mouse that were positive for αSMA staining (**B**). (**C**) Representative kidney sections of both groups showing αSMA staining in pink, while green color indicates autofluorescence. (**D**, **E**) Quantitative realtime analysis of *P2ry6* mRNA levels (**D**) normalized to *actb* as well as collagen 1 (*Col1a1*) mRNA levels (**E**). Abbreviations: αSMA= as smooth muscle actin

worldwide are affected by CKD, making it the 12th leading cause of death globally, and it is projected to become the 5th leading cause by 2040 [35]. CKD is characterized by excessive accumulation of extracellular matrix (ECM), primarily produced by activated myofibroblasts, which largely originate from PDGFR-β-positive interstitial fibroblasts [4, 6, 10]. Understanding the molecular mechanisms driving fibroblast activation is crucial for developing targeted antifibrotic therapies.

In this study, we investigated the role of $G_{q/11}$-protein coupled P2Y receptors in renal interstitial fibroblasts and their contribution to experimental kidney fibrosis. Among all P2Y receptors analyzed, only $P2Y_1$ and $P2Y_6$ were enriched in renal interstitial cells, with $P2Y_6$ being selectively upregulated in experimental fibrosis models. Strikingly, pharmacological interference in the $P2Y_6$ signaling during fibrosis progression in mice significantly attenuated fibrosis outcome in mice. During the process of preparing this manuscript for peer review submission, submission but after publishing the key data of this manuscript on a preprint server [36], Figurek et al. independently reported that UDP-$P2Y_6$ mediated signaling promotes fibroblasts activation and renal fibrosis progression [37], highlighting the physiological relevance of P2 signaling in interstitial cell biology and further underscore its potential as a therapeutic target. While Figurek et al. present conceptually similar findings regarding UDP–$P2Y_6$ signaling in interstitial fibroblasts, our study provides substantial additional value by offering isoform-resolved spatial mapping of $G_{q/11}$-coupled P2Y receptors, macrophage involvement, and by extending the antifibrotic efficacy of $P2Y_6$ inhibition to a clinically relevant adenine-induced nephropathy model.

Due to the low mRNA copy number as well as low protein abundance of many (G protein-coupled) receptors, we opted for the highly specific mRNA hybridization technique RNAscope to explore localization of the $G_{q/11}$ protein-coupled P2Y receptors $P2Y_1$ (*P2ry1*), $P2Y_2$ (*P2ry2*), $P2Y_4$ (*P2ry4*), and $P2Y_6$ (*P2ry6*) in renal interstitial fibroblasts that we labeled with a PDGFR-β (*Pdgfrb*) probe (Fig. 1). $P2Y_1$ was detected in glomerular cells, proximal tubular cells, urothelium and PDGFR-β-positive interstitial cells. Consistent with the literature reporting $P2Y_2$ activity in (proximal) tubular cells, mesangial cells and arterioles, we observed $P2Y_2$ localization in epithelial cells, with increasing expression towards the medulla [15, 20]. $P2Y_4$ expression was minimal, while $P2Y_6$ was the only receptor strongly enriched in PDGFR-β-positive fibroblasts, with additional localization in proximal tubules. Basal $P2Y_6$ expression in

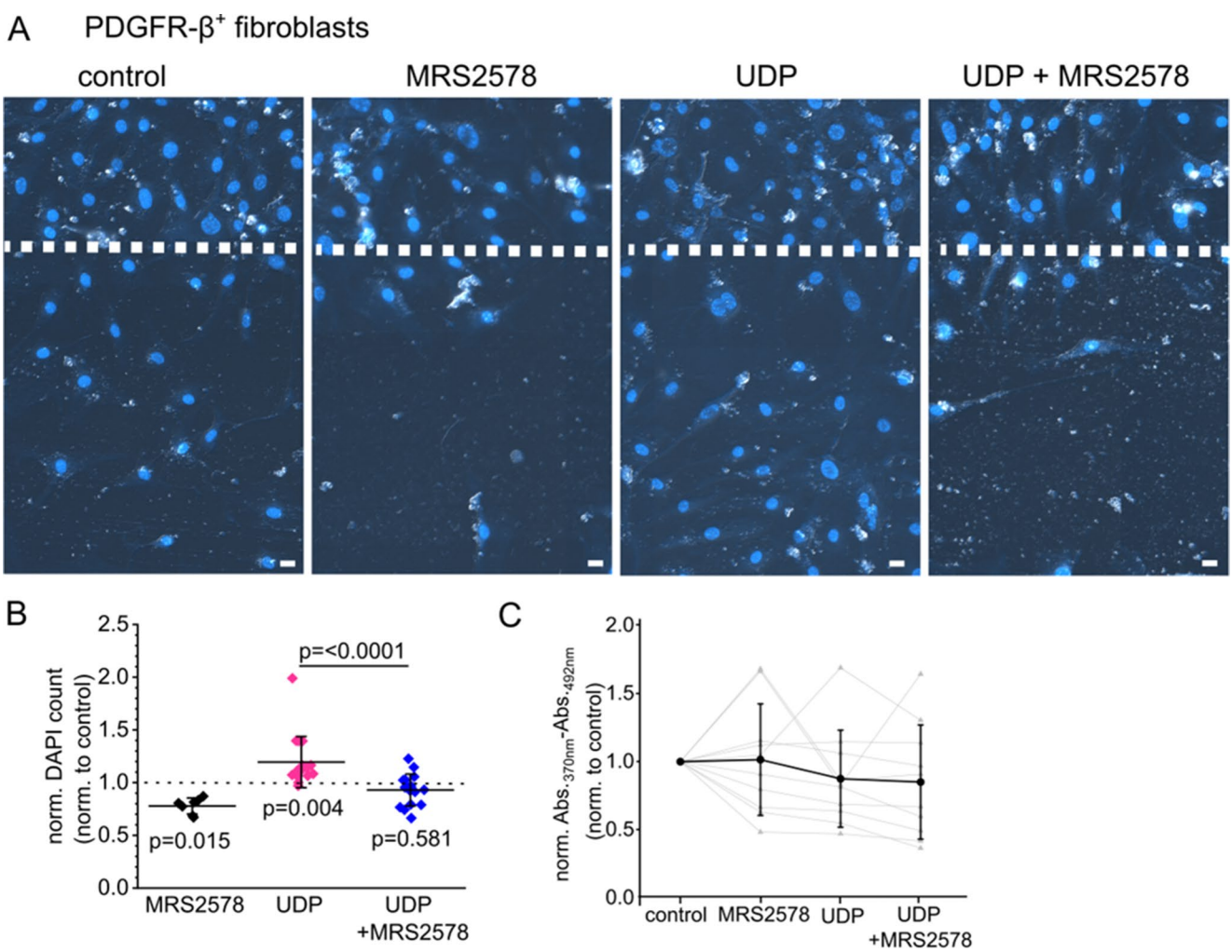

Fig. 5 UDP promotes cell migration of cultured renal fibroblasts via $P2Y_6$ activation. (**A**) Representative pictures of cultured FACS-sorted murine PDGFR-β-positive renal fibroblasts 48h after wounding and subsequent stimulation with either 30 µM UDP or 30 µM UDP + 5 µM of the $P2Y_6$ inhibitor MRS2578. Nuclei were counterstained using HOE33342 indicated in blue. (**B**) Migration was evaluated by automatic counting of migrated nuclei per area and is depicted as a percentage compared with the control (stippled line). (**C**) Proliferation of cells was evaluated using an BrdU ELISA in the absence and/or presence of 30 µM UDP and 5 µM MRS2578. Grey symbols represent one condition within independent experiments. Lines connect related conditions within one independent experiment. Black values and lines represent means ± STD. Abbreviattions: FACS=fluorescence-activated cell sorting, PDGFR-β = platelet-derived growth factor β, UDP= Uridine Diphosphate.

PDGFR-β-positive interstitial cells - but not proximal tubular expression, whose $P2Y_6$ functionality has been reported previously in rat proximal tubular cells by others [20] - was also observed in the work of Figurek et al., who analyzed single cell RNA-sequencing databases [37].

Because mRNA and protein expression do not necessarily correlate, we confirmed functional P2Y receptor activity in FACS-sorted, cultured renal fibroblasts: superfusion of FACS-sorted cultured renal fibroblasts with different nucleotides induced Ca^{2+}-transients (Fig. 2). Specific pharmacological interference of either $P2Y_1$ using MRS2179 or $P2Y_6$ using MRS2578 did significantly reduce ADP- or UDP-mediated Ca^{2+}-signals although Ca^{2+}-signals were not completely abolished supporting receptor specificity despite partial cross-activation at high nucleotide concentrations [38]. Of note, we did not detect unspecific blockage of other nucleotide signals using MRS2179 or MRS2578 confirming the specificity of the used compounds (Supplementary Fig. 2). The distinct expression profile of the different P2Y receptors was also evident in RNAscope experiments using the same FACS-sorted cell lines (Supplementary Fig. 1) where $P2Y_4$ expression was low and $P2Y_6$, $P2Y_1$ and $P2Y_2$ expression was abundant suggesting that although the components of the nucleotide signaling pathway are redundantly expressed, each P2Y seems to have a distinct role in cell regulation.

While our test of functionality was performed using cultured fibroblasts, Figurek and colleagues also observed

UDP-$P2Y_6$ mediated signaling using freshly cut slices from the kidneys of transgenic mice expressing the fluorescent Ca^{2+}-reporter GCaMP6s, indicating that the core signaling mechanism is highly reproducible and underscoring the robustness of the UDP-$P2Y_6$ axis across distinct experimental systems.

Although upregulation of $P2Y_6$ expression was likewise reported in the various disease models analyzed by Figurek et al. (ischemia–reperfusion injury, unilateral ureter obstruction, folic acid nephropathy), the pronounced expression of $P2Y_6$ in F4/80-positive interstitial macrophages observed in our study (Fig. 3) represents a conceptually novel finding. This dual localization in PDGFR-β-positive fibroblasts and macrophages suggests that $P2Y_6$ may coordinate fibrotic remodeling through both stromal and immune compartments, adding an important layer of complexity to the $P2Y_6$ fibrosis axis.

We wondered how these findings in mice translate to a human kidney injury and attempted immunofluorescent labeling of $P2Y_6$ in murine and human tissue samples. Attempts to validate $P2Y_6$ protein expression by immunofluorescence were inconclusive, likely due to low receptor abundance. However, searches in commonly available human databases verified our own observations since $P2Y_6$ upregulation in fibroblasts was also observed in an single-cell transcriptomics approach with acute kidney injury samples [39] as well as in single cells RNA sequencing data from the KPMP kidney tissue atlas (https://atlas.kpmp.org) indicating a common cross-species phenomena in mice and men.

Given the expression of $P2Y_6$ in the renal interstitium, the question arose whether inhibition of $P2Y_6$-signaling using the specific inhibitor MRS2578 might affect fibrosis progression in experimental fibrosis models (Fig. 4). The most striking observation of our study was that pharmacological inhibition of $P2Y_6$ with MRS2578 using i.p. injections three times a week significantly reduced fibrosis in adenine-induced nephropathy, as evidenced by decreased αSMA^+ myofibroblast area and lower expression of fibrotic markers such as collagen I (*Col1a1*). In contrast, renal function, as assessed by blood urea nitrogen and serum creatinine levels, remained unchanged between MRS2578-treated and vehicle-treated groups (Supplementary Fig. 7). The dissociation between reduced fibrosis and preserved renal function may reflect a temporal delay between structural improvement and functional recovery, as well as the limited sensitivity of conventional renal function markers, particularly in mild injury settings. Furthermore, $P2Y_6$ signaling appears to primarily regulate inflammatory and fibrotic pathways, which may not translate into measurable changes in glomerular filtration unless tissue damage reaches a more advanced stage. Importantly, reduced fibrosis may nevertheless improve the capacity for renal recovery following subsequent injury.

Our data align closely with the findings reported by Figurek and colleagues, further underscoring the reproducibility of $P2Y_6$ involvement in another model of renal fibrosis. In addition to demonstrating similar expression patterns, Figurek et al. employed a global $P2Y_6$ knockout model to confirm attenuation of fibrosis, thereby supporting the conclusion that the antifibrotic effects are indeed mediated by $P2Y_6$ rather than off-target actions of the pharmacological inhibitor MRS2578. However, given the dual expression of $P2Y_6$ in PDGFR-β-positive interstitial cells and F4/80-positive macrophages, our experiments cannot definitively distinguish whether the observed effects originate from fibroblasts, macrophages, or both.

This limitation highlights the need for future studies employing cell-type–specific deletion strategies. Nonetheless, both studies collectively emphasize the therapeutic potential of targeting $P2Y_6$ -signaling in chronic kidney disease.

It is intriguing to speculate how interstitial fibroblasts, which predominantly express diphosphate-sensitive receptors $P2Y_1$ and $P2Y_6$, are activated under physiological conditions. While ATP release is well characterized — occurring via exocytosis, ATP-permeable channels such as connexin 43 (*Cx43*) and pannexin 1 (*Panx1*), or passively from dying cells — the mechanisms governing UTP or UDP release are less understood, though release from necrotic cells appears likely [16, 17]. Studies in rat intestinal epithelial cells revealed negligible basal extracellular nucleotide levels, yet mechanical injury triggered rapid release of ATP and UDP, but not ADP or UTP [40], suggesting distinct nucleotide-release dynamics. Figurek et al. provided compelling evidence that pyrimidine metabolism is highly active in the proximal tubule and that the key pyrimidine salvage enzyme cytidine deaminase, which converts cytidine to uridine to maintain the cellular UDP pool, is upregulated in chronic kidney disease. Cultured human proximal tubular HK-2 cells also displayed increased extracellular UDP concentrations following injury, consistent with proximal-tubule–derived UDP serving as a paracrine signal for interstitial effector cells such as fibroblasts and macrophages [37].

What are the consequences of UDP release for effector cells? Our data indicate that UDP enhances fibroblast migration in wound-healing assays, whereas no effect on fibroblast proliferation was observed (Fig.5). This suggests that PDGFR-β-positive fibroblasts may migrate toward sites of UDP release. Conversely, macrophages exhibited reduced migration under the same conditions. Previous studies have shown that macrophages are attracted by UDP but subsequently activate and differentiate [33].

It is intriguing to speculate, that $P2Y_6$ signaling may also influence macrophage infiltration indirectly by modulating pericyte contraction and detachment, leading to modified capillary flow, and localized barrier disruption. These changes could create "hot spots" of damage that facilitate macrophage entry. As pericytes transition into myofibroblasts during chronic injury, loss of pericyte coverage and deposition of stiff extracellular matrix may permanently alter capillary geometry and generate hypoxic niches that favor pro-fibrotic macrophage phenotypes. As mentioned above, future studies will be required to dissect the relative contributions of PDGFR-β-positive fibroblasts and F4/80-positive macrophages to the fibrotic phenotype in a cell-type–specific manner.

Interestingly, Bar et al., [33] observed that $P2Y_6$-null mice are viable and phenotypically indistinguishable from wild-type mice in terms of growth and fertility. Yet, they exhibit impaired UDP responses in macrophages, endothelial cells, and vascular smooth muscle [33]. The same group also implicated $P2Y_6$ to be a therapeutic target to regulate cardiac hypertrophy since the $P2Y_6$ gene knockout is associated with a macrocardia phenotype and amplified pathological cardiac hypertrophy in mice [41]. Beyond renal and cardiovascular disease, recent evidence suggests $P2Y_6$ as potential immunotherapy target since increased production of UDP attracts immunosuppressive macrophages through its receptor $P2Y_6$ while pharmacological interference of immunosuppressive macrophages by MRS2578 promoted responsiveness to immunotherapies in otherwise resistant pancreatic ductal adenocarcinoma and melanoma models [42].

In summary, this study demonstrates that $P2Y_6$ is expressed under control conditions in renal interstitial fibroblasts and, upon activation, promotes cell migration. In CKD, $P2Y_6$ is additionally expressed by infiltrating macrophages. Pharmacological blockade with MRS2578 markedly reduced fibrotic lesions, highlighting its therapeutic potential. Our study is limited by the absence of $P2Y_6$ protein level verification since a specific antibody to verify $P2Y_6$ protein expression is lacking. Secondly, our study is based on murine models, although single-cell RNA sequencing data suggest conservation of the pathophysiology in humans. Nonetheless, functional validation in human tissue or organoid models is needed. Third, the pharmacological inhibitor MRS2578, while selective, may have off-target effects, and its pharmacokinetics and safety profile remain insufficiently characterized for clinical translation which should be addressed in future studies. Together with the study from Figurek et al. [37], our study highlights $P2Y_6$ inhibition as beneficial, positioning $P2Y_6$ as a promising candidate for further investigation into fibrotic signaling and targeted therapy development for CKD.

Methods

Ethical Approval

All animal experiments were conducted in accordance with Directive 2010/63/EU of the European Parliament and of the Council on the protection of animals used for scientific purposes. The experiments also comply with the animal ethics checklist of this journal. All experiments were approved the local councils for animal care (Regierung von Unterfranken) according to the German law for animal care.

Mice

Wildtype mice in a BL/6J background were used in the studies with experimental kidney fibrosis. For FACS-sorting of PDGFR-β-positive renal cells, murine kidneys from tamoxifen-induced PDGFR-β $Cre^{ERT/2}$ mTmG mice [43] that express a membranous GFP under control of the PDGFR-β-promotor were used. All mice were kept on 12 : 12 h light-dark cycle, controlled temperature levels (22 °C ± 2 °C) and humidity (55% ±10%).Animals were fed a standard rodent chow (0.6% NaCl; Ssniff, Soest, Germany) with free access to autoclaved tap water.

Adenine-induced nephropathy

Adenine-induced fibrosis was generated in adult male mice at the age of 6–16 weeks. An 0.2% adenine-containing diet (altromin Spezialfutter GmbH, Germany) was fed continuously for 3 weeks. Experiments were performed after exactly 3 weeks (3-week adenine). To assess P2ry expression in healthy and fibrotic kidneys (Fig. 3 and Supplementary Fig. 3), paraffin-embedded tissue samples and cDNA from Fuchs et al. were re-examined, thereby avoiding additional animal experimentation and ensuring that the procedure is fully compliant with the 3R guidelines for animal research [3]. To assess the effect of $P2Y_6$ inhibitor using MRS2578 during fibrosis progression (Fig. 4), animals receiving adenine diet and i.p. injection of vehicle (control group) were compared to animals receiving adenine diet and i.p. injections of MRS2578 (treatment group). Fibrosis progression was assessed using αSMA staining's as primary outcome measure. Experimental unit was considered as a single animal. Sample size was eight animals per group, no animals were excluded from analysis. Randomization was achieved by distributing littermates equally between experimental groups, while blinding was implemented solely through automated image analysis to ensure objective assessment. Confounders were minimized by using randomization, blinding, standardized procedures, and consistent environmental conditions throughout the experiment.

(Reversible) unilateral ureteral obstruction (UUO)

For analysis of UUO kidneys, paraffin-embedded tissue and cDNA samples from Fuchs et al. were re-examined, thereby avoiding additional animal experimentation and ensuring that the procedure is fully compliant with the 3R guidelines for animal research [3]. In short, ureteral ligation using a suture was performed close to the right kidney through a small abdominal incision under inhalation anesthesia. Five days after the procedure, mice were killed and perfused for RNAscope or kidneys were removed for mRNA quantification. For reversible unilateral ureteral obstruction (rUUO) kidneys, the right kidney of female mice was clipped at the age of 6–16 weeks by making a small incision in the abdomen under anesthesia using 0.5 mg*kg^{-1} medetomidine, 5 mg/kg, midazolam, and 0.05 mg*kg^{-1}, fentanyl at day 0. In addition, 200 mg*kg^{-1} paracetamol and 25 mg*kg^{-1} tramadol was administered subcutaneously for pain relief. To awaken the mice from anesthesia, they were injected subcutaneously with 2.5 mg*kg^{-1} atipamezole, 0.5 mg*kg^{-1} flumazenil, and 1.2 mg*kg^{-1} naloxone. The clip was replaced more caudally at day 2 and removed at day 4, whereafter mice were left to recover for two weeks. Injection of vehicle was performed i.p. three times a week. Left, undamaged kidneys were used as internal controls while the clamped (right) kidney was considered treatment group. Sample size was nine animals per group. No predefined termination criteria were met during the experimentation. To assess *P2ry* expression in healthy and fibrotic kidneys (Fig. 3), successful fibrosis progression was assessed by immunohistological staining and automated analysis of the primary outcome measure αSMA-positive area. Animals that showed fibrotic lesions of 2-fold or higher were included in the analysis of *P2ry* expression ($n=6$). In two more kidneys no RNAscope signal could be detected, since background signals were too high for inclusion. Randomization was achieved by distributing littermates equally between experimental groups, while blinding was implemented solely through automated image analysis to ensure objective assessment. Confounders were minimized by using randomization, blinding, standardized procedures, and consistent environmental conditions throughout the experiment.

Drug Treatments

For in vivo use, MRS2578 (Selleckchem Chemicals LLC, Houston, USA) was prepared at a concentration of 5 mg*mL^{-1} in a vehicle consisting of 30% propylene glycol, 5% Tween 80 and 65% D5W according to the manufacturer's instructions and administered i.p. at a concentration of 10 mg*kg^{-1} BW three times a week. Treatment started one day before start of the experiment while control animals received solventinjections intraperitoneally (2 µl*kg^{-1} BW) at the same time points. For in vitro use, a stock solution of 5 mM MRS2578 was prepared in DMSO and used at 5 µM concentration.

Determination of mRNA expression by real-time PCR

Total RNA was isolated from murine kidneys after perfusion with 0.9% NaCl containing heparin. Kidneys were snap frozen in liquid nitrogen, total RNA was extracted using the RNeasy plus mini kit (Quiagen, Hilden, Germany). The purity and integrity of the RNA were verified spectroscopically using a Nano Drop spectrometer (Life Technologies GmbH, Darmstadt, Germany). For qPCR, cDNA was generated from 1 µg total RNA by reverse transcription using M-MLV Reverse Transcriptase (Life Technologies GmbH, Darmstadt, Germany) according to the protocol provided. To quantify mRNA expression, real-time PCR was performed using the LightCycler Takyon® No ROX SYBR 2X MasterMix (Eurogentec, Seraing, Belgium) and the LightCycler 96 SW instrument (Roche Diagnostics, Mannheim, Germany). Transcript levels were normalized to the expression of the housekeeping protein β-Actin (*Actb*). Primers (Eurofins, Munich, Germany) are listed in Table 1.

In situ hybridization via RNAscope®

RNAscope analysis was performed on kidneys perfused with 0.9% NaCl followed by fixation with 3% paraformaldehyde solution. The fixed tissue was dehydrated, embedded in paraffin, and cut into 5 µm sections with a microtome as described previously [3]. Target mRNAs were hybridized and visualized using the RNAscope® Multiplex Fluorescent v2 kit (Advanced Cell Diagnostics, Hayward, CA, USA) following the manufacturer's instructions (Wang et al., 2012). Signal detection was performed with TSA Vivid dyes 570 and 650 (Bio-Techne, Wiesbaden, Germany) and the Opal 780 fluorophore (Akoya Biosciences, Marlborough,

Table 1 Primer sequences used for qPCR

Target gene	Sequence (5´to 3´), fwd	Sequence (5´to 3´), rev	Amplicon size (bp)
Actb	CCACCGATCCACACAGAGTACTT	GACAGGATGCAGAAGGAGATTACTG	98
P2ry1	GAGGTGCCTTGGTCGGTTG	CGGCAGGTAGTAGAACTGGAA	159
P2ry2	GGGTGACCACTGGCCATTTA	TGCTGCAGTAGAGGTTGGTG	60
P2ry6	GTGAGGATTTCAAGCGACTGC	TCCCCTCTGGCGTAGTTATAGA	208
Col1a1	CTGACGCATGGCCAAGAAGA	ATACCTCGGGTTTCCACGTC	91

MA). Nuclei were counterstained with DAPI included in the Multiplex Fluorescent v2 kit. Sections were mounted using ProLong™ Gold Antifade Mountant (Thermo Fisher Scientific, Waltham, MA, USA) and stored at 4 °C until further analysis. The RNAscope® probes employed are listed in Table 2.

All RNAScope® images were taken with an Axio Observer.Z1 microscope (Zeiss, Jena, Germany) using the Plan-Apochromat 20x/0.8 objective and the Colibri7 as light source. Fluorescent images were captured with the Axiocam 506 mono. Filters used were the filter set 43-Cy3 (EX BP 545/25; EM BP 605/70), filter set 50-Cy5 shift free (EX BP 640/30; EM BP 690/50), filter set 96 HE BFP (EX BP 390/40; EM BP 450/40) and filter set 115-Cy7 (EX BP 710/87; EM BP 814/91) (Zeiss). For detail fluorescent images, the Apotome.2 system (Zeiss) was used to take 10 to 15 z-stacked images, which were merged using maximum projection. Overviews were generated by stitching tiles taken at 20x magnification. Images in the same figure were taken with the same light intensities, exposure times and displayed with identical image modifications.

FACS sorting and cell culture of murine renal fibroblasts

Murine kidneys from tamoxifen-induced PDGFR-β Cre$^{ERT/2}$ mTmG mice were perfused with 0.9% NaCl to remove blood and 0.1 mg*mL^{-1} collagenase II-containing (Merck KGaA, Germany) in DMEM medium (PAN-Biotech GmbH, Germany). Kidneys were harvested, decapsulated, cut into small pieces and transferred to a tube with 1 mg*mL^{-1} collagenase II-containing in DMEM. Enzymatic digestion took place at 37 °C at 800 rpm in a tube shaker for 60 min. To ensure active collagenase activity, kidney suspension was centrifuged at 3000 rpm for 3 min, supernatant was replaced by fresh collagenase solution three times during the incubation period. Remaining kidney fragments were dissociated by gentle pipetting using a cut 1 mL-tip. Digestion was stopped by addition of DMEM medium containing 10% fetal calf serum (FCS) (Capricorn Scientific GmbH, Germany). Cells were washed three times with PBS and resuspended for FACS sorting in PBS containing 1% FCS. Shortly before sorting, cells were transferred into a FACS tube containing a 30 µm sieve. GFP-positive cells were sorted using a BD FACSAria™ Fusion Flow Cytometer into a tube containing DMEM + 10% FCS and kept on ice until cells were washed with cell culture medium (DMEM, low glucose, GlutaMax (Gibco) + 15% FCS (Gibco), 1% Insulin-Transferrin-Selenium, 1%Pen/Strep + 0,1% Amphotericin B) and incubated at 37 °C and 5% CO_2. Splitting of cells was done at 80–90 confluency using accutase.

Table 2 RNAscope probes used for in situ hybridization

RNAscope®- Probe	Cat No.	RNAscope®- Probe	Cat No.
Mm-P2ry6-C1	314,241	Mm-P2ry2-C3	406,051-C3
Mm-Pdgfrb-C3	411,381-C3	Mm-P2ry4-C2	406,081-C2
Mm-Pdgfrb-C1	411,381		
Mm-P2ry1-C2	406,061-C2	Mm-Adgre1-C2	460,651-C2

Scratch assay of FACS-sorted murine renal fibroblasts

A total of 500,000 cells were seeded into 35 mm culture dishes and grown in standard cell culture medium until reaching confluency. Cells were then serum-starved for 24 h in medium lacking fetal calf serum (FCS). Linear wounds approximately 1 mm wide were generated in the monolayer using sterile 20 µL pipette tips. After scratching, cells were washed to remove debris and dead cells, and 2 mL of fresh serum-free medium was added, supplemented with either 30 µM UDP and/or 5 µM MRS2578, or left untreated (control). Each dish contained three scratch areas. Images of the same positions were captured immediately after scratching (0 h) and at 48 h using a Zeiss Axio Observer. Z1 microscope equipped with an AxioCam 305 mono camera and a 10×/0.25 objective (Zeiss, Jena, Germany). At 48 h, cells were stained by washing with Ringer solution followed by incubation for 5 min in Ringer containing 1 µM Hoechst 33,342. Migration was quantified by counting nuclei within the wound area using ZEN Intellesis software (Zeiss, Jena, Germany) using a thresholding approach. For each dish, counts from the three scratches were averaged and expressed as a fraction relative to untreated controls. Experiments were performed using at least three different FACS-sorted cell lines.

Proliferation of FACS-sorted murine fibroblasts

A total of 2,000 cells were seeded into each well of a 96-well plate and grown in standard cell culture medium until 30 µM UDP and/or 5 µM MRS2578 was added for 24 h. BrdU incorporation was assessed using the colorimetiric BrdU cell proliferation ELISA (Roche) according to the manual provided by the manufacturer. Each condition was tested four times, and the mean value of these four measurements is shown as one n. The experiment was repeated at least three times using different FACS-derived cell lines.

Videomicrosopic Ca^{2+}-measurements using Fura2-AM

For videomicroscopic Fura2 Ca^{2+}-imaging, FACS-sorted renal fibroblasts were split at least one day prior to experiment onto glass coverslips and incubated for

30 min at 37 °C with 2 µM Fura2-AM and Powerload (Roche) in Ringer solution containing (in millimoles) 5 Hepes, 145 NaCl, 5 Glucose, 0.4 KH_2PO_4,1.6 K_2HPO_4,1 $MgCl_2$, 1.3 $CaCl_2$. Afterwards, cells were rinsed, and glass cover slips was inserted onto a perfusion chamber and measured with the Zeiss Axio Oberver.Z1 using an Fluar 40x/1.3 oil objective (Zeiss, Jena, Germany). Cells were continuously superfused with Ringer solution containing different agonists or antagonists as indicated. Perfusion speed was 2 $mL*min^{-1}$. Fura2 was excited at 340 and 380 nm with a LAMBDA DG-4 lamp (World Precision Instruments) using 340/40 and 387/15 BP filters and exposure times of 250 and 100 ms, respectively. Fura2 emission at 510 nm was recorded using a AxioCam 305 mono (Zeiss) and BS FT 409 and BP 510/90 filters. Sampling interval was 5 s. 340/380 emission ratio after background subtraction of cell-free region-of-interest is indicated for each cell (grey lines) within one dish. Measurements of non-responsive cells were not further analyzed as those cells were either dead or did not express necessary P2Y-receptors. For each dish, the mean basal ratios and the mean maximal ratio under agonist simulation of responsive cells was determined. Graphical summaries represent means per dish. Each experiment was at least repeated on three different days with multiple FACS-sorted primary cell lines.

Immunofluorescence

To detect immunofluorescence signals, kidneys were perfusion-fixed with 3% paraformaldehyde and after dehydration in an ascending methanol and isopropanol series embedded in paraffin. Staining was performed on 5 µm sections. Sections were deparaffinized and blocked with 5% bovine serum albumin in phosphate-buffered saline solution and incubated with mouse α-smooth muscle actin antibody (ab7187, Abcam, Cambridge, UK) at 4 °C overnight. After three washes with phosphate-buffered saline solution, sections were incubated with respective Cy3-conjugated secondary antibody (Dianova, Hamburg, Germany) and mounted with Glycergel (Agilent, Waldbronn, Germany). Overviews of one whole kidney cross-section per mouse were taken by stitching tiles with the Zeiss Axio Oberver.Z1 using an 20x/0.8 oil objective (Zeiss, Jena, Germany) equipped with an AxioCam 305 mono camera, a LAMBDA DG-4 lamp (World Precision Instruments) and filter set 43-Cy3 (EX BP 545/25; EM BP 605/70) to detect α-smooth muscle actin and filter set 38 HE (EX BP 470/40; FT 495, EM BP 525/50) to detect autofluorescence. Images in the same figure were taken with the same light intensities, exposure times and displayed with identical image modifications.

Image Analysis

Automated image analysis (Intellesis software, Zeiss ZEN) was used to determine the cortical mRNA expression levels of PDGFR-β, P2Y6, and F4/80. Segmentation was performed by background subtraction with rolling ball method (radius 10), considering a threshold range between defined minimum intensity values (PDGFR-β: 350, P2Y6: 200, F4/80: 400) and the maximum pixel intensity (16383) with a tolerance level of 3%. No size exclusion criteria were applied during the analysis to ensure that all detected RNAscope signals were taken into account. For the detection of cell nuclei, segmentation was performed using global thresholding (DAPI intensities between 1500 and 16383). The area of the detected expression intensities of PDGFR-β, P2Y6, and F4/80 was normalized to the area of the detected cell nuclei. Automated analysis of cortical αSMA^+ area normalized to EGFP-positive autofluorescence area was analyzed using a thresholding approach using the ZEN Intellesis software. Data is depicted as cortical area per mouse. Image analysis software was funded by the Deutsche Forschungsgemeinschaft (DFG, German Research Foundation) - Projektnummer 471,535,567.

Statistical analyses

All data are presented as mean ± SD. Data were analyzed using Origin 2024 (OriginLab Corporation, Northampton, Massachusetts, USA). In Fura2-measurements, statistical testing of agonist-signals versus baseline was performed using a paired ttest. To analyze statistical significance between different agonist stimulations, a one-way ANOVA with Tukey's correction and mean comparisons was used. In the experimental murine fibrosis models, a Wilcoxon rank sum test was performed to analyze statistical difference except for rUUO kidneys, were contralateral and rUUO kidney were compared with a Wilcoxon signed-rank test. p values and group sizes are stated in the results section. If stated, a *post hoc* Bonferroni correction was applied for multiple testing, otherwise $p \leq 0.05$ was considered statistically significant.

Supplementary Information The online version contains supplementary material available at https://doi.org/10.1007/s00424-026-03187-8.

Acknowledgements The authors would like to thank Ines Tegtmeier and Justina Rötsch for their expert technical assistance. This work was funded by the Deutsche Forschungsgemeinschaft (DFG, German Research Foundation), project number 509149993, TRR 374. The discussion is in part based upon data generated by the Kidney Precision Medicine Project. Accessed December 8th, 2025. https://www.kpmp.org. The Kidney Precision Medicine Project (KPMP) is supported by the National Institute of Diabetes and Digestive and Kidney Diseases (NIDDK) through the following grants: U01DK133081, U01DK133091, U01DK133092, U01DK133093,

U01DK133095, U01DK133097, U01DK114866, U01DK114908, U01DK133090, U01DK133113, U01DK133766, U01DK133768, U01DK114907, U01DK114920, U01DK114923, U01DK114933, U24DK114886, UH3DK114926, UH3DK114861, UH3DK114915, and UH3DK114937. We gratefully acknowledge the essential contributions of our patient participants and the support of the American public through their tax dollars.

Author contributions LMS, KB and ALF designed the experiments. LMS, AP, AS, MLT, BF, and ALF conducted the experiments and performed the data analyses. LMS, RW, ALF, and KB were responsible for the interpretation of the results. LMS and ALF drafted the main manuscript, and ALF prepared figures. KB and RW critically revised the manuscript for important intellectual content and provided substantial conceptual and editorial input. All authors reviewed, commented on, and approved the final version of this manuscript. All authors agree to be accountable for all aspects of the work, ensuring the accuracy and integrity of the research.

Funding Open Access funding enabled and organized by Projekt DEAL. This work was funded by the Deutsche Forschungsgemeinschaft (DFG, German Research Foundation), project number 509149993, TRR 374.

Data availability The datasets generated during and/or analyzed during the current study are available at urn: nbn: de: bvb:355-epub-786001.

Declarations

Data Sharing Statement The datasets generated during and/or analyzed during the current study are available at urn: nbn: de: bvb:355-epub-786001.

Competing interests The authors declare no competing interests.

Clinical Trial Number not applicable.

References

1. Huang R, Fu P, Ma L (2023) Kidney fibrosis: from mechanisms to therapeutic medicines, Signal Transduct. Target Ther 8:129. https://doi.org/10.1038/s41392-023-01379-7
2. B.D. Humphreys, Mechanisms of Renal Fibrosis
3. Fuchs MAA, Broeker KAE, Schrankl J, Burzlaff N, Willam C, Wagner C, Kurtz A (2021) Inhibition of transforming growth factor β1 signaling in resident interstitial cells attenuates profibrotic gene expression and preserves erythropoietin production during experimental kidney fibrosis in mice. Kidney Int 100:122–137. https://doi.org/10.1016/j.kint.2021.02.035
4. Buchtler S, Grill A, Hofmarksrichter S, Stöckert P, Schiechl-Brachner G, Rodriguez Gomez M, Neumayer S, Schmidbauer K, Talke Y, Klinkhammer BM, Boor P, Medvinsky A, Renner K, Castrop H, Mack M (2018) Cellular Origin and Functional Relevance of Collagen I Production in the Kidney. J Am Soc Nephrol 29:1859–1873. https://doi.org/10.1681/ASN.2018020138
5. Gomez IG, Duffield JS (2011) The FOXD1 lineage of kidney perivascular cells and myofibroblasts: functions and responses to injury. Kidney Int Suppl 4(2014):26–33. https://doi.org/10.1038/kisup.2014.6
6. Humphreys BD, Lin S-L, Kobayashi A, Hudson TE, Nowlin BT, Bonventre JV, Valerius MT, McMahon AP, Duffield JS (2010) Fate tracing reveals the pericyte and not epithelial origin of myofibroblasts in kidney fibrosis. Am J Pathol 176:85–97. https://doi.org/10.2353/ajpath.2010.090517
7. Klinkhammer BM, Djudjaj S, Kunter U, Palsson R, Edvardsson VO, Wiech T, Thorsteinsdottir M, Hardarson S, Foresto-Neto O, Mulay SR, Moeller MJ, Jahnen-Dechent W, Floege J, Anders H-J, Boor P (2020) Cellular and Molecular Mechanisms of Kidney Injury in 2,8-Dihydroxyadenine Nephropathy. J Am Soc Nephrol 31:799–816. https://doi.org/10.1681/ASN.2019080827
8. Broeker KAE, Fuchs MAA, Schrankl J, Kurt B, Nolan KA, Wenger RH, Kramann R, Wagner C, Kurtz A (2020) Different subpopulations of kidney interstitial cells produce erythropoietin and factors supporting tissue oxygenation in response to hypoxia in vivo. Kidney Int 98:918–931. https://doi.org/10.1016/j.kint.2020.04.040
9. Falke LL, Gholizadeh S, Goldschmeding R, Kok RJ, Nguyen TQ (2015) Diverse origins of the myofibroblast—implications for kidney fibrosis. Nat Rev Nephrol 11:233–244. https://doi.org/10.1038/nrneph.2014.246
10. Kuppe C, Ibrahim MM, Kranz J, Zhang X, Ziegler S, Perales-Patón J, Jansen J, Reimer KC, Smith JR, Dobie R, Wilson-Kanamori JR, Halder M, Xu Y, Kabgani N, Kaesler N, Klaus M, Gernhold L, Puelles VG, Huber TB, Boor P, Menzel S, Hoogenboezem RM, Bindels EMJ, Steffens J, Floege J, Schneider RK, Saez-Rodriguez J, Henderson NC, Kramann R (2021) Decoding myofibroblast origins in human kidney fibrosis. Nature 589:281–286. https://doi.org/10.1038/s41586-020-2941-1
11. Wang Y-Y, Jiang H, Pan J, Huang X-R, Wang Y-C, Huang H-F, To K-F, Nikolic-Paterson DJ, Lan H-Y, Chen J-H (2017) Macrophage-to-Myofibroblast Transition Contributes to Interstitial Fibrosis in Chronic Renal Allograft Injury. J Am Soc Nephrol 28:2053–2067. https://doi.org/10.1681/ASN.2016050573
12. Meng X-M, Nikolic-Paterson DJ, Lan HY (2016) TGF-β: the master regulator of fibrosis. Nat Rev Nephrol 12:325–338. https://doi.org/10.1038/nrneph.2016.48
13. Cappelli C, Tellez A, Jara C, Alarcón S, Torres A, Mendoza P, Podestá L, Flores C, Quezada C, Oyarzún C, San R, Martín (2020) The TGF-β profibrotic cascade targets ecto-5'-nucleotidase gene in proximal tubule epithelial cells and is a traceable marker of progressive diabetic kidney disease. Biochim Biophys Acta Mol Basis Dis 1866:165796. https://doi.org/10.1016/j.bbadis.2020.165796
14. Forst A-L, Olteanu VS, Mollet G, Wlodkowski T, Schaefer F, Dietrich A, Reiser J, Gudermann T (2016) Mederos y Schnitzler, U. Storch, Podocyte Purinergic P2X4 Channels Are Mechanotransducers That Mediate Cytoskeletal Disorganization. J Am Soc Nephrol 27:848–862. https://doi.org/10.1681/ASN.2014111144
15. Menzies RI, Tam FW, Unwin RJ, Bailey MA (2017) Purinergic signaling in kidney disease. Kidney Int 91:315–323. https://doi.org/10.1016/j.kint.2016.08.029

16. Jankowski J, Perry HM, Medina CB, Huang L, Yao J, Bajwa A, Lorenz UM, Rosin DL, Ravichandran KS, Isakson BE, Okusa MD (2018) Epithelial and Endothelial Pannexin1 Channels Mediate AKI. J Am Soc Nephrol 29:1887–1899. https://doi.org/10.1681/ASN.2017121306
17. Price GW, Chadjichristos CE, Kavvadas P, Tang SCW, Yiu WH, Green CR, Potter JA, Siamantouras E, Squires PE, Hills CE (2020) Blocking Connexin-43 mediated hemichannel activity protects against early tubular injury in experimental chronic kidney disease. Cell Commun Signal 18:79. https://doi.org/10.1186/s12964-020-00558-1
18. Lu D, Insel PA (2014) Cellular mechanisms of tissue fibrosis. 6. Purinergic signaling and response in fibroblasts and tissue fibrosis. Am J Physiol Cell Physiol 306:C779–C788. https://doi.org/10.1152/ajpcell.00381.2013
19. Burnstock G, Evans LC, Bailey MA (2014) Purinergic signalling in the kidney in health and disease. Purinergic Signal 10:71–101. https://doi.org/10.1007/s11302-013-9400-5
20. Kraus K, Skoczynski M, Brötsch N, Burzlaff J, Leipziger M, Schiffer M, Büttner-Herold B, Buchholz (2014) P2Y2R and Cyst Growth in Polycystic Kidney Disease. J Am Soc Nephrol. https://doi.org/10.1681/ASN.0000000000000416
21. Roberts VS, Cowan PJ, Alexander SI, Robson SC, Dwyer KM (2014) The role of adenosine receptors A2A and A2B signaling in renal fibrosis. Kidney Int 86:685–692. https://doi.org/10.1038/ki.2014.244
22. Müller CE, Namasivayam V (2021) Recommended tool compounds and drugs for blocking P2X and P2Y receptors. Purinergic Signal 17:633–648. https://doi.org/10.1007/s11302-021-09813-7
23. Harding SD, Armstrong JF, Faccenda E, Southan C, Alexander SPH, Davenport AP, Spedding M, Davies JA (2024) The IUPHAR/BPS Guide to PHARMACOLOGY in 2024. Nucleic Acids Res 52:D1438–D1449. https://doi.org/10.1093/nar/gkad944
24. Menzies RI, Howarth AR, Unwin RJ, Tam FWK, Mullins JJ, Bailey MA (2015) Inhibition of the purinergic P2X7 receptor improves renal perfusion in angiotensin-II-infused rats. Kidney Int 88:1079–1087. https://doi.org/10.1038/ki.2015.182
25. Rennert L, Zschiedrich S, Sandner L, Hartleben B, Cicko S, Ayata CK, Meyer C, Zech A, Zeiser R, Huber TB, Idzko M, Grahammer F (2018) P2Y2R Signaling Is Involved in the Onset of Glomerulonephritis. Front Immunol 9:1589. https://doi.org/10.3389/fimmu.2018.01589
26. van der Giet M, Giebing G, Tolle M, Schmidt S (2002) The Role of P2Y Receptors in the Control of Blood Pressure. Drug News Perspect 15:640–646. https://doi.org/10.1358/dnp.2002.15.10.740237
27. Hillman KA, Woolf AS, Johnson TM, Wade A, Unwin RJ, Winyard PJD (2004) The P2X7 ATP receptor modulates renal cyst development in vitro. Biochem Biophys Res Commun 322:434–439. https://doi.org/10.1016/j.bbrc.2004.07.148
28. Therkildsen JR, Christensen MG, Tingskov SJ, Wehmöller J, Nørregaard R, Praetorius HA (2019) Lack of P2X7 Receptors Protects against Renal Fibrosis after Pyelonephritis with α-Hemolysin-Producing Escherichia coli. Am J Pathol 189:1201–1211. https://doi.org/10.1016/j.ajpath.2019.02.013
29. Zhang R, Su K, Yang L, Duan H, Tang L, Tang M, Zhao M, Ye N, Cai X, Jiang X, Li N, Peng J, Zhang X, Tang L, Qiu Q, Chen L, Wu W, Hu J, Ma L, Ye H (2024) Discovery of a Potent, Orally Active, and Long-Lasting P2X7 Receptor Antagonist as a Preclinical Candidate for Delaying the Progression of Chronic Kidney Disease. J Med Chem 67:17472–17496. https://doi.org/10.1021/acs.jmedchem.4c01395
30. Lee JW, Chou C-L, Knepper MA (2015) Deep Sequencing in Microdissected Renal Tubules Identifies Nephron Segment-Specific Transcriptomes. J Am Soc Nephrol 26:2669–2677. https://doi.org/10.1681/ASN.2014111067
31. Nishida M, Sato Y, Uemura A, Narita Y, Tozaki-Saitoh H, Nakaya M, Ide T, Suzuki K, Inoue K, Nagao T, Kurose H (2008) P2Y6 receptor-Galpha12/13 signalling in cardiomyocytes triggers pressure overload-induced cardiac fibrosis. EMBO J 27:3104–3115. https://doi.org/10.1038/emboj.2008.237
32. Nishiyama K, Nishimura A, Shimoda K, Tanaka T, Kato Y, Shibata T, Tanaka H, Kurose H, Azuma Y-T, Ihara H, Kumagai Y, Akaike T, Eaton P, Uchida K, Nishida M (2022) Redox-dependent internalization of the purinergic P2Y6 receptor limits colitis progression. Sci Signal 15:eabj0644. https://doi.org/10.1126/scisignal.abj0644
33. Bar P-J, Guns J, Metallo D, Cammarata F, Wilkin J-M, Boeynams H, Bult B, Robaye (2008) Knockout mice reveal a role for P2Y6 receptor in macrophages, endothelial cells, and vascular smooth muscle cells. Mol Pharmacol 74:777–784. https://doi.org/10.1124/mol.108.046904
34. Garcia RA, Yan M, Search D, Zhang R, Carson NL, Ryan CS, Smith-Monroy C, Zheng J, Chen J, Kong Y, Tang H, Hellings SE, Wardwell-Swanson J, Dinchuk JE, Psaltis GC, Gordon DA, Glunz PW, Gargalovic PS (2014) P2Y6 receptor potentiates pro-inflammatory responses in macrophages and exhibits differential roles in atherosclerotic lesion development. PLoS ONE 9:e111385. https://doi.org/10.1371/journal.pone.0111385
35. Foreman KJ, Marquez N, Dolgert A, Fukutaki K, Fullman N, McGaughey M, Pletcher MA, Smith AE, Tang K, Yuan C-W, Brown JC, Friedman J, He J, Heuton KR, Holmberg M, Patel DJ, Reidy P, Carter A, Cercy K, Chapin A, Douwes-Schultz D, Frank T, Goettsch F, Liu PY, Nandakumar V, Reitsma MB, Reuter V, Sadat N, Sorensen RJD, Srinivasan V, Updike RL, York H, Lopez AD, Lozano R, Lim SS, Mokdad AH, Vollset SE, Murray CJL (2018) Forecasting life expectancy, years of life lost, and all-cause and cause-specific mortality for 250 causes of death: reference and alternative scenarios for 2016-40 for 195 countries and territories. Lancet 392:2052–2090. https://doi.org/10.1016/S0140-6736(18)31694-5
36. Süß LM, Petzendorfer A, Firmke B, Süß A, Warth R, Broeker KA-E, Forst A-L, Inhibition of (interstitial) P2Y6 receptors attenuates renal fibrosis progression, bioRxiv, Figurek N, Jankovic S, Kollar M, Kaminska I, Sakhi A, Rinaldi PE, Cippà B, Robaye AM (2026) Hall Pyrimidinergic calcium signaling links tubular metabolism to fibrosis in kidney disease. Nat Commun (2026). https://doi.org/10.1038/s41467-026-69602-x
37. Figurek A, Jankovic J, Kollar S, Kaminska M, Sakhi I, Rinaldi A, Cippà PE, Robaye B, Hall AM (2026) Pyrimidinergic calcium signaling links tubular metabolism to fibrosis in kidney disease. Nat Commun. https://doi.org/10.1038/s41467-026-69602-x
38. Jacobson KA, Ivanov AA, de Castro S, Harden TK, Ko H (2009) Development of selective agonists and antagonists of P2Y receptors. Purinergic Signal 5:75–89. https://doi.org/10.1007/s11302-008-9106-2
39. Hinze C, Kocks C, Leiz J, Karaiskos N, Boltengagen A, Cao S, Skopnik CM, Klocke J, Hardenberg J-H, Stockmann H, Gotthardt I, Obermayer B, Haghverdi L, Wyler E, Landthaler M, Bachmann S, Hocke AC, Corman V, Busch J, Schneider W, Himmerkus N, Bleich M, Eckardt K-U, Enghard P, Rajewsky N (2022) Schmidt-Ott, Single-cell transcriptomics reveals common epithelial response patterns in human acute kidney injury. Genome Med 14:103. https://doi.org/10.1186/s13073-022-01108-9
40. Nakamura T, Murata T, Hori M, Ozaki H (2013) UDP induces intestinal epithelial migration via the P2Y6 receptor. Br J Pharmacol 170:883–892. https://doi.org/10.1111/bph.12334
41. Clouet S, Di Pietrantonio L, Daskalopoulos E-P, Esfahani H, Horckmans M, Vanorlé M, Lemaire A, Balligand J-L, Beauloye

C, Boeynaems J-M, Communi D (2016) Loss of Mouse P2Y6 Nucleotide Receptor Is Associated with Physiological Macrocardia and Amplified Pathological Cardiac Hypertrophy. J Biol Chem 291:15841–15852. https://doi.org/10.1074/jbc.M115.684118

42. Scolaro T, Manco M, Pecqueux M, Amorim R, Trotta R, van Acker HH, van Haele M, Shirgaonkar N, Naulaerts S, Daniluk J, Prenen F, Varamo C, Ponti D, Doglioni G, Ferreira Campos AM, Fernandez Garcia J, Radenkovic S, Rouhi P, Beatovic A, Wang L, Wang Y, Tzoumpa A, Antoranz A, Sargsian A, Di Matteo M, Berardi E, Goveia J, Ghesquière B, Roskams T, Soenen S, Voets T, Manshian B, Fendt S-M, Carmeliet P, Garg AD, DasGupta R, Topal B, Mazzone M (2024) Nucleotide metabolism in cancer cells fuels a UDP-driven macrophage cross-talk, promoting immunosuppression and immunotherapy resistance. Nat Cancer 5:1206–1226. https://doi.org/10.1038/s43018-024-00771-8
43. Gerl K, Nolan KA, Karger C, Fuchs M, Wenger RH, Stolt CC, Willam C, Kurtz A, Kurt B (2016) Erythropoietin production by PDGFR-β(+) cells, Pflugers Arch. 468:1479–1487. https://doi.org/10.1007/s00424-016-1829-2